

J. Lee and A. P. Reeves. "Segmentation of individual ribs from low-dose chest CT," In *Medical Imaging 2010: Computer-aided Diagnosis*, N. Karssemeijer, R. M. Summers, eds., vol. 7624, pp. 76243J, 2010.

<http://dx.doi.org/10.1117/12.844565>

Copyright 2010 Society of Photo-Optical Instrumentation Engineers.

One print or electronic copy may be made for personal use only. Systematic or multiple reproduction, duplication of any material in this paper for a fee or for commercial purposes, or modification of the content of the paper are prohibited.

Segmentation of Individual Ribs from Low-dose Chest CT

Jaesung Lee and Anthony P. Reeves

School of Electrical and Computer Engineering
Cornell University, Ithaca, NY, USA

ABSTRACT

Segmentation of individual ribs and other bone structures in chest CT images is important for anatomical analysis, as the segmented ribs may be used as a baseline reference for locating organs within a chest as well as for identification and measurement of any geometric abnormalities in the bone. In this paper we present a fully automated algorithm to segment the individual ribs from low-dose chest CT scans. The proposed algorithm consists of four main stages. First, all the high-intensity bone structure present in the scan is segmented. Second, the centerline of the spinal canal is identified using a distance transform of the bone segmentation. Then, the seed region for every rib is detected based on the identified centerline, and each rib is grown from the seed region and separated from the corresponding vertebra. This algorithm was evaluated using 115 low-dose chest CT scans from public databases with various slice thicknesses. The algorithm parameters were determined using 5 scans, and remaining 110 scans were used to evaluate the performance of the segmentation algorithm. The outcome of the algorithm was inspected by an author for the correctness of the segmentation. The results indicate that over 98% of the individual ribs were correctly segmented with the proposed algorithm.

Keywords: Ribs, segmentation, X-ray computed tomography

1. INTRODUCTION

The segmentation of individual ribs in chest CT images may serve as a first step in an anatomical analysis. The labeled ribs may be used as a baseline reference for locating organs and other features within the chest.¹ Further, the segmentation of the ribs provides an opportunity for detection and evaluation of geometric abnormalities in the bone. Typically an individual has 24 ribs, 12 on each side of the chest. Manual identification of individual ribs is a time consuming task on a 3D volumetric CT data.

In the paper we present a fully automated algorithm to segment the individual ribs from a low-dose chest CT scan. Main challenges for automatically segmenting individual ribs are their proximity to a corresponding vertebra and the intensity variation within a rib due to bone marrow and bone density variations. Further, noise present in low-dose CT images may interfere with the segmentation.

There has been considerable interest in algorithm for segmenting the rib cage. Staal et al.² presented a method to segment and label individual ribs in CT. Their method first identified image primitives and construct rib centerline using the primitives. The full ribs were then grown from the constructed centerlines. Klinder et al.³ used a rib cage model constructed from their training set. Their algorithm then detects the centerlines of the ribs in a CT image using the pre-established model. Shen et al.⁴ introduced a rib tracing algorithm using dynamic programming based on the geometrical shape of the ribs. Kiraly et al.⁵ proposed a tracing-based visualization of ribs. Their method traced the centerline of each rib and performs straightening of individual ribs to aid the visualization of the ribs.

In related work Kang et al.⁶ applied 3D image techniques to segment the proximal femur in CT data. Their method used 3D region-growing with local adaptive threshold followed by morphological operation to obtain the segmentation. The bone segmentation has also been explored in other modalities such as MR. Lorigo et al.⁷ used a method based on active contour model to segment the tibia and femur in MR images of knees.

Further author information: (Send correspondence to Jaesung Lee)
E-mail: jl569@cornell.edu, Telephone: 1 607 255 0963

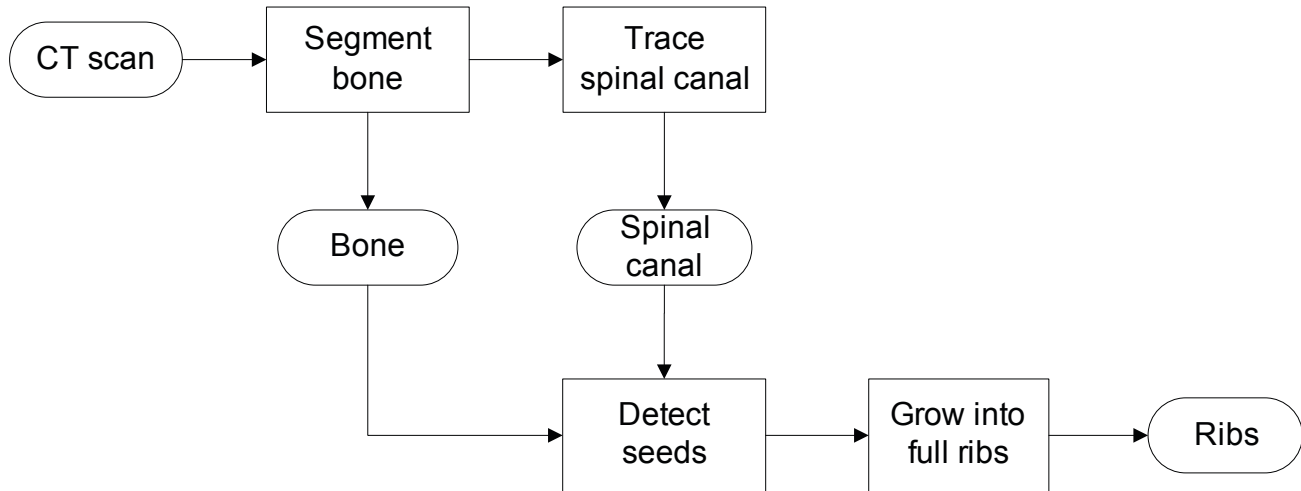


Figure 1. Flowchart for the proposed method. Bone and spinal canal are found first and used to detect the seed for every rib. Stepwise approach yields segmentation of ribs as well as spinal canal and other bones.

Most previously-proposed rib segmentation methods use a rib cage model constructed from a set of training cases. While this approach works well in many cases, it may fail to perform robustly for a wide range of 3D image data due to variation in bone's appearance. Our work focuses on the robust rib segmentation algorithm that does not rely heavily on a pre-established rib cage model.

2. METHOD AND MATERIALS

The algorithm to segment individual ribs employs a stepwise approach and consists of four stages. The entire algorithm is outlined with a flowchart in Figure 1. First, all the bone structure present in the scan is segmented. Second, the centerline of the spinal canal is identified. Then, based on the identified centerline and the segmented bone, a seed region for every rib is detected. Finally, individual ribs are grown from each seed and separated from the corresponding vertebra.

2.1 Bone Segmentation

The outcome of bone segmentation includes all the bone structures visible in the chest CT including the rib cage, scapula, sternum, and clavicle (Figure 2). First, each image is filtered with a 3x3 mean filter to reduce noise present in the data. The entire CT scan is then thresholded at 175 HU to capture high-intensity bone structures. Any connected component that is smaller than 4500 mm³ in volume is considered as noise and is removed from the segmentation.

The intensity and volume thresholds for this stage were determined empirically from experimenting with five cases. The intensity threshold was set to include all bones in the scan and high enough so that the hollow region of the rib corresponds to approximately one third of the external rib diameter. The volume threshold was chosen to exclude high-intensity noise components.

2.2 Spinal Canal Tracing

The center of spinal canal is traced from the segmented bone structure. Figure 3 shows the extracted center line of a spinal canal in sagittal view. A seed point is automatically identified from the projection of the lowest 25 mm of image slices. Then, the entire canal is traced upward using an iterative algorithm starting at the seed point. Each iteration of the algorithm involves an image slice (I_i) and the image slice above (I_{i-1}). The tracing algorithm is outlined in the following:

1. Find an initial seed point for the lowest image.

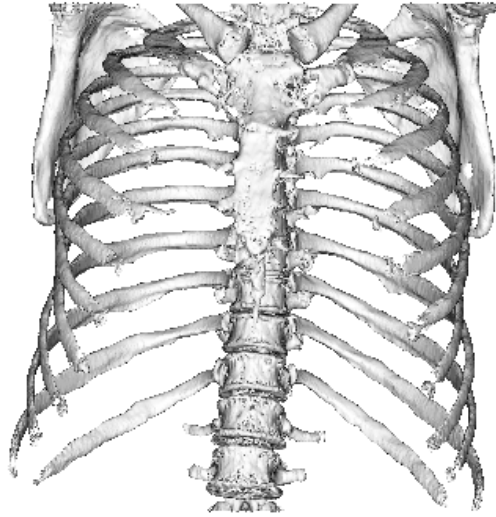


Figure 2. Coronal visualization of segmented bones. The bone segmentation includes all the bones visible in the chest CT and is used as a basis for segmenting the spinal canal and individual ribs.



Figure 3. Tracing of spinal canal. The traced line is shown in a sagittal projection of the spine. The extracted center line is used to locate the seed points for individual ribs.

2. Compute a 2D distance transform in image I_{i-1} .
3. Find a point in I_{i-1} that is close to the previous point in I_i and is at a maximum in the distance transform.
4. Repeat 1 and 2 for all images in the scan.
5. The canal's center line is formed using all identified points.

The distance transform is performed within a subregion around the spine, as opposed to the entire image, to increase the efficiency of the algorithm.

2.3 Rib Segmentation

From the segmentation in the first stage which includes high-intensity bone region, each rib is attached to a vertebra, and the entire rib cage and the spine appear as one connected component on the segmented bones. To segment each rib, it is necessary to separate the rib from the corresponding vertebra. Figure 4a illustrates our approach for growing a rib. A seed region is found for each rib, and the rib is traced inward toward the vertebra.

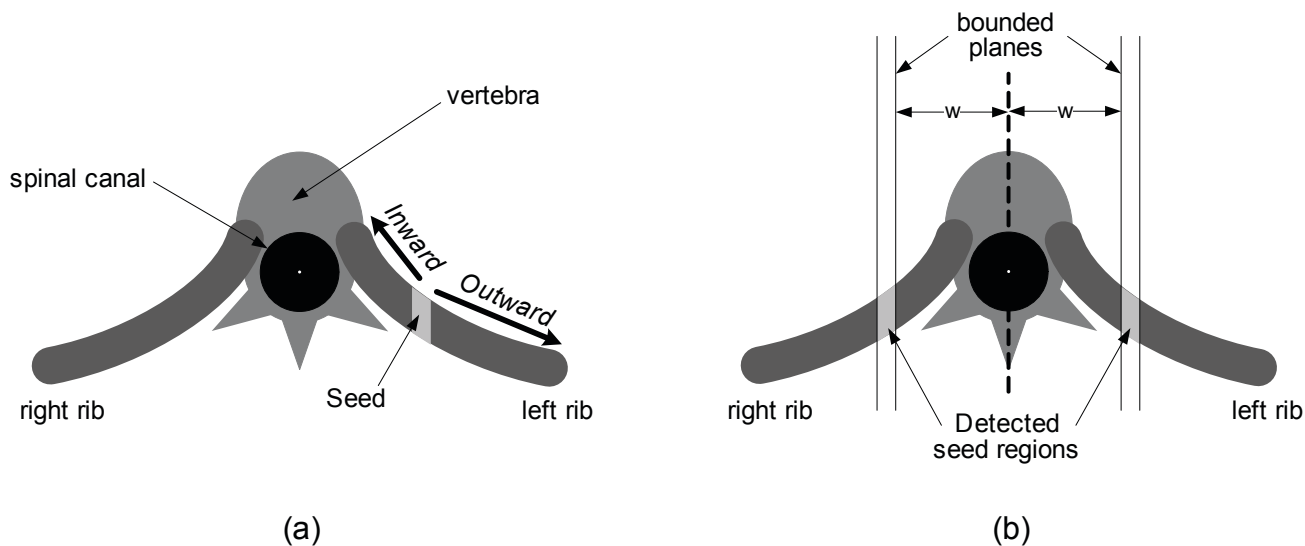


Figure 4. Rib segmentation algorithm. (a) To separate the rib from the vertebra, the rib is grown in both directions from a seed. (b) A seed is identified for every rib using bounded planes established on both sides of a spinal canal's center point.

The outward portion of the rib from the seed region may be segmented simply using a connected component analysis.

2.3.1 Seed detection

An illustration for detecting a seed region is shown in Figure 4b. A seed region for each rib is identified by screening the segmented image region at a distance w to the left and to the right of the spinal canal's centerline. The value of w is set large enough so that the planes do not touch a vertebra. Within each plane, any voxel that belongs to a bone as segmented in the previous section is found, and a 3D connected component is grown within the plane starting at that voxel.

Two criteria are used to determine if a detected seed region actually belongs to a rib. First its volume must be greater than a pre-established threshold, and second the component must span through the entire width of bounded plane. Once it meets both criteria the starting region is labeled with a unique label. The algorithm for detecting a seed region of ribs is outlined in Algorithm 1.

Algorithm 1 Detecting a rib seed

```

 $P \leftarrow$  vertical planes at  $\pm w$  from center
label  $\leftarrow$  0
for all  $v(x, y, z)$  do
  if  $v(x, y, z) \in \text{bone}$  and  $v(x, y, z) \in P$  then
     $R = \text{Grow}(v(x, y, z), P)$  /* grow within P */
    if  $R$  crosses  $P$  and  $\text{Volume}(R) \geq \text{Min\_volume}$  then
      /* rib seed detected */
      label  $\leftarrow$  label + 1
       $v(x, y, z) \leftarrow$  label
    end if
  end if
end for

```

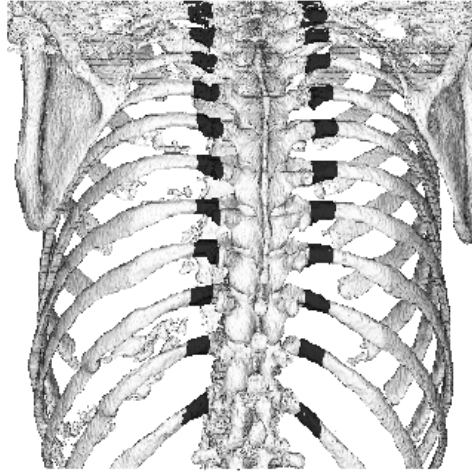


Figure 5. Detected rib seed regions. Coronal posterior visualization of the segmented bones is shown, with the rib seeds highlighted in black.

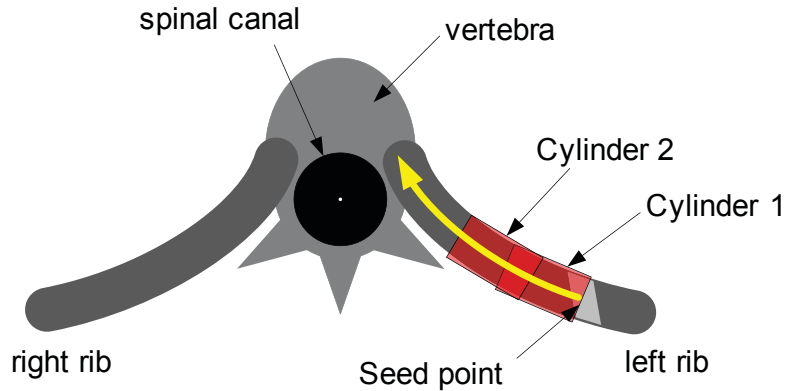


Figure 6. Tracing the rib toward vertebra. Starting at a seed, cylindrical template is iteratively advanced along the rib.

2.3.2 Rib growing

Every detected seed region is grown into full rib and given a unique label. The outer portion of the rib is segmented using 3D region growing, by iteratively adding any connected voxels. When growing the rib outward, 8-connectivity is used in the 3D image space.

The inner portion of the rib is traced by fitting a hollow cylindrical volume along the rib, as illustrated in Figure 6. Starting at the seed region, a cylindrical volume is iteratively advanced until it reaches the expected length of the inner rib portion. Each iteration determines the direction of the cylinder by finding the highest correlation to the pre-filtered CT image (Equation 1). The expected length is determined by taking the distance between the seed region and the center of spinal canal.

$$Direction = \operatorname{argmax}_{dir} \left(\sum_{x,y,z \in cyl_{dir}} I(x,y,z) \right), \quad (1)$$

where cyl_{dir} is a hollow cylindrical template, and $I(x,y,z)$ is the CT image intensity at (x,y,z) .

For tracing along the rib, a hollow cylinder is used as a template since bone marrow appears in low intensity when compared to the bone surface. The parameters for the cylindrical template include diameter d , thickness

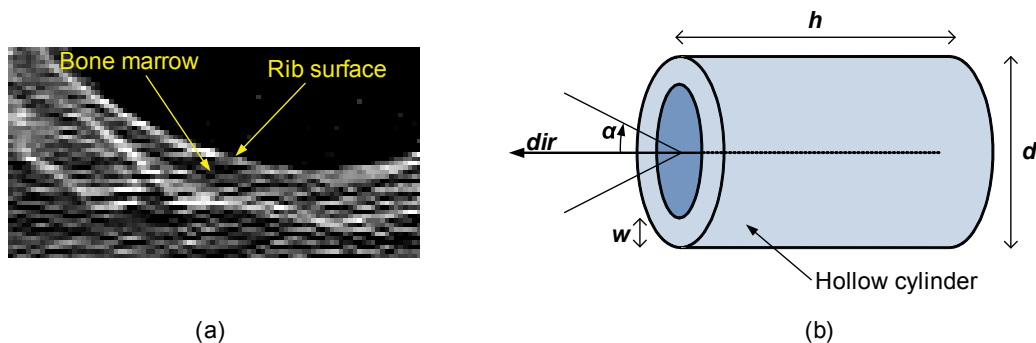


Figure 7. Cylindrical template for rib tracing. (a) Bone marrow appears in low intensity compared to the surface, and the hollow cylinder is used to trace the rib. (b) Parameters for the hollow cylinder template include diameter, thickness, height, and search angle.

Table 1. Distribution for number of segmented ribs

Segmented ribs	Scans with 24 ribs	Scans with 22 ribs
24	86 (81%)	-
23	8 (8%)	-
22	12 (11%)	4 (100%)
Total	106	4

w , height h , and search angle α (Figure 7). The values of d and w are adjusted adaptively for each rib by finding the values that yield the highest correlation for the first iteration. Other parameters, h and α , were determined empirically using five training cases.

The cylinder height h was set so that the cylinder can be traced along the curved trajectory of a rib and to be insensitive to image noise. The search angle was set differently for anterior and posterior directions. A small search angle was used toward posterior direction since the ribs should curve toward anterior direction as it approaches the vertebra. The value of h was set to 10 mm, and α was set to 2 and 45 degrees for posterior and anterior directions, respectively.

2.4 Experiment

Each of the CT scans was carefully inspected by one of the authors to establish the number of ribs present in each scan. The fully automated method was then run to segment the individual ribs. For each case, the outcome was visually inspected to confirm correct segmentation. The algorithm's performance was evaluated by comparing the number of segmented ribs to the number established by the inspector.

The dataset included 115 whole-lung chest CT scans from public databases.^{8,9} From the dataset, 5 scans were used for determining algorithm parameters, and the remaining 110 scans were used to evaluate the algorithm performance. All of the scans were taken with low radiation dose (120kV-140kV, 40mAs-80mAs) with slice thicknesses varying from 1.25mm to 2.5mm. In-plane resolution of the scans ranged from 0.55mm x 0.55mm to 0.82mm x 0.82mm. Upon visual inspection of the scans, 106 scans had all 24 ribs present in the scan, and 4 scans had only 22 ribs due to truncation.

3. RESULTS

Examples of segmentation outcomes are shown in Figure 8 as 3D visualizations. A total of 2632 ribs were present in 110 CT scans, and the algorithm correctly segmented 2600 ribs (98.8%). All ribs other than the highest and lowest ribs were successfully segmented; of the 32 ribs that were not correctly segmented, 6 were the highest ribs, and 26 were the lowest ribs.

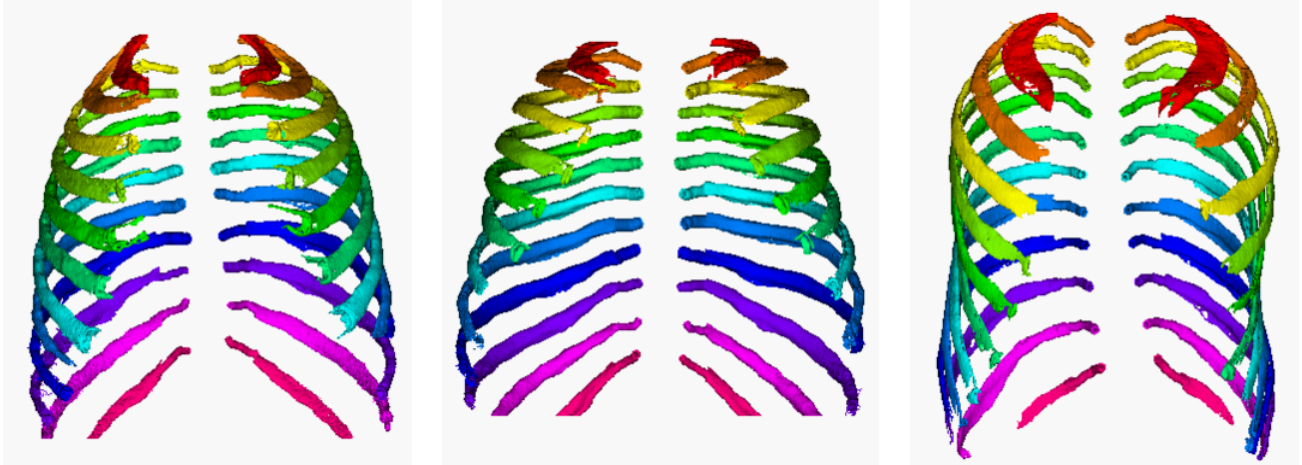


Figure 8. 3D visualizations of segmented and labeled ribs. The segmentations from three different CT scans are shown, where each rib is labeled with a unique color.

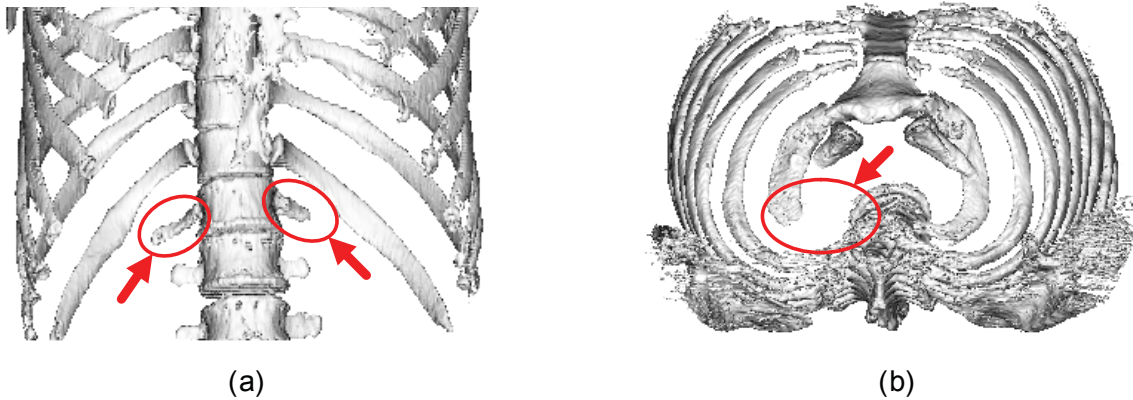


Figure 9. Examples of missed ribs (pointed with arrows). (a) A coronal visualization of the lower rib cage is shown. The lowest ribs with short length were often missed. (b) An axial visualization of the rib cage is shown. The top-most left rib was truncated in the CT image and missed by the algorithm.

The distribution of cases is shown in Table 1, where the cases are categorized into two groups according to the number of ribs present in the scan (24 and 22). For each group, the cases are divided according to the number of ribs that are correctly segmented. There were 90 cases where all ribs present in the scan were correctly segmented.

4. DISCUSSION

The presented method is fully automatic without any need for manual intervention. A stepwise approach allows for segmentation of other bone structures and the spinal canal as well as individual ribs. The algorithm was capable of segmenting at least 22 ribs in all cases. Further, total number of ribs present in all 110 cases was 2632, of which 2600 (98.8%) were successfully segmented.

The main cause of the missed ribs was the short length of the lowest ribs (Figure 9a). Other missed ribs were due to the top-most ribs that were partly truncated (Figure 9b). In both situations the algorithm failed to detect the seed since the bounded planes did not intersect the rib.

The segmented rib cage may be used to establish a common chest frame of reference that defines a common coordinate system for the chest region.¹ Individually-labeled ribs may be further used to define more precise

reference points within such a chest frame and establish non-linear transformation of a given CT scan to a chest reference frame. Future work will focus on refining a reference frame scheme based on entire rib cage.

5. CONCLUSION

Segmentation of the individual ribs from a 3D image data may be used as a baseline reference for locating anatomical structures and features. In this paper, a fully automated method for segmentation of individual ribs was presented. This algorithm locates the roots of ribs and segments full ribs from the detected roots. The algorithm was evaluated with 110 low-dose chest CT scans, and the preliminary results show that it performs well as more than 98% of the ribs have been successfully segmented.

6. ACKNOWLEDGMENT

This work was supported in part by a grant from Carestream Health, Inc. Dr. Reeves is a co-inventor on patents and other pending patents relating to evaluation of diseases of the chest including measurement of nodules. Some of these, which are owned by Cornell Research Foundation (CRF) are non-exclusively licensed to General Electric and they receive royalties from CRF pursuant to Cornell policy, which in turn is consistent with the Bayh-Dole Act.

REFERENCES

- [1] Lee, J., Biancardi, A., Reeves, A., Yankelevitz, D., and Henschke, C., "Estimation of anatomical locations using standard frame of reference in chest CT scans," *Proceedings of IEEE Engineering in Medicine and Biology Conference*, 5809–5812 (2009).
- [2] Staal, J., van Ginneken, B., and Viergever, M., "Automatic rib segmentation and labeling in computed tomography scans using a general framework for detection, recognition and segmentation of objects in volumetric data," *Medical Image Analysis* **11**(1), 35–46 (2007).
- [3] Klinder, T., Lorenz, C., von Berg, J., Dries, S., Bulow, T., and Ostermann, J., "Automated model-based rib cage segmentation and labeling in CT images," *Lecture Notes in Computer Science* **4792**, 195 (2007).
- [4] Shen, H., Liang, L., Shao, M., and Qing, S., "Tracing based segmentation for the labeling of individual rib structures in chest CT volume data," *Lecture Notes in Computer Science*, 967–974 (2004).
- [5] Kiraly, A., Qing, S., and Shen, H., "A novel visualization method for the ribs within chest volume data," *Proceedings of SPIE Medical Imaging* **6141**, 614108 (2006).
- [6] Kang, Y., Engelke, K., and Kalender, W., "A new accurate and precise 3-D segmentation method for skeletal structures in volumetric CT data," *IEEE Transactions on Medical Imaging* **22**(5), 586–598 (2003).
- [7] Lorigo, L., Faugeras, O., Grimson, W., Keriven, R., and Kikinis, R., "Segmentation of bone in clinical knee MRI using texture-based geodesic active contours," *Lecture Notes in Computer Science*, 1195–1204 (1998).
- [8] Reeves, A. P., Biancardi, A. M., Yankelevitz, D. F., Fotin, S., Keller, B. M., Jiraptnakul, A., and Lee, J., "A public image database to support research in computer aided diagnosis," *Proceedings of IEEE Engineering in Medicine and Biology Conference*, 3715–3718 (2009).
- [9] Reeves, A., Biancardi, A., Apanasovich, T., Meyer, C., MacMahon, H., van Beek, E., Kazerooni, E., Yankelevitz, D., McNitt-Gray, M., McLennan, G., et al., "The lung image database consortium (LIDC) a comparison of different size metrics for pulmonary nodule measurements," *Academic radiology* **14**(12), 1475–1485 (2007).